$^{40}Ar/^{39}Ar$ chronology and geochemistry of high-K volcanic rocks in the Mangkang basin, Tibet

ZHANG Huihua[1], HE Huaiyu[2], WANG Jianghai[3,1] & XIE Guanghong[1]

1. Guangzhou Institute of Geochemistry, Chinese Academy of Sciences, Guangzhou 510640, China;
2. Institute of Geology and Geophysics, Chinese Academy of Sciences, Beijing 100029, China;
3. College of Life Sciences, Sun Yat-Sen University, Guangzhou 510275, China
Correspondence should be addressed to Wang Jianghai (email: wangjh@gig.ac.cn)

Received July 5, 2003

Abstract Our two newly obtained high-quality $^{40}Ar/^{39}Ar$ ages suggest that the high-K volcanic rocks of the Lawuxiang Formation in the Mangkang basin, Tibet were formed at 33.5 ± 0.2 Ma. The tracing of elemental and Pb-Sr-Nd isotopic geochemistry indicates that they were derived from an EM2 enriched mantle in continental subduction caused by transpression. Their evidently negative anomalies in HFSEs such as Nb and Ta make clear that there is an input of continental material into the mantle source. The high-K rocks at 33.5 ± 0.2 Ma in the Mangkang basin may temporally, spatially and compositionally compare with the early one of two-pulse high-K rocks in eastern Tibet distinguished by Wang J. H. et al., implying that they were formed in the same tectonic setting.

Keywords: Cenozoic high-K volcanic rocks, $^{40}Ar/^{39}Ar$ chronology, Mangkang basin, Tibet.

DOI: 10.1360/03yd0125

One belt of Cenozoic discontinuous arc-shaped high-K magmatism occurs along the Jinsha-Red River Shear (JRRS) zone[1—6], and was generated during large-scale SE-treading extrusion of Indochina induced by the Indo-Asian collision[7—9] (fig. 1(a)). The Mangkang basin in the northern segment of the JRRS zone (fig. 1(b)) is a narrow pull-apart basin, which was developed on the Mesozoic basement after the basement underwent long-term uplift and exhumation[7,10] and was controlled by NNW-treading thrusting at two margins of the basin. The earliest strata in this basin were developed at Cretaceous, and are a set of brick-red calcareous quartz sandstones, lithic sandstones, calcareous siltstones and mudstones with gypsum interlayers. The Eocene strata are a set of purple-red clastic rocks with a thickness of ~400 meters, which are composed of conglomerates and pebble-bearing sandstones. The early Oligocene strata are a layer of conglomerates. Subsequently, a set of grey-yellow glutenites with sandstone interlayers was appeared. After that, a set of high-K volcanic rocks occurred. The volcanic rocks, together with lower Oligocene grey-yellow clastic rocks constitute the Lawuxiang Formation (fig. 2). The Tertiary clastic rocks were slightly deformed.

The Bureau of Geology and Mineral Resources (Tibet)[11] had carried out mapping of the 1 : 200000 regional geology in the Mangkang area, and divided the high-K rocks into the Neogene Lawuxiang Formation. Lai S. C.[12,13] proposed that the high-K rocks belong to a shoshonitic series, and may be derived from a crust-mantle mixing layer at the bottom of a

Copyright by Science in China Press 2005

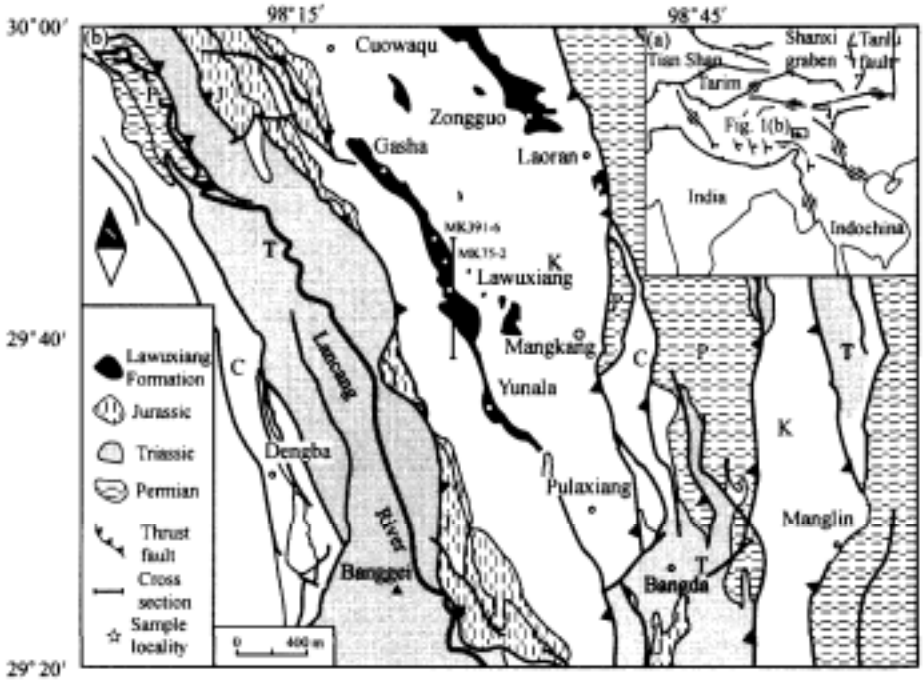

Fig. 1. Simplified geologic map in the Mangkang area, Tibet, illustrating the tectonic setting and sampling localities of high-K rocks.

thickened crust on the basis of petrological and petrochemical observations. Until now, no report is presented on systematic chronological and geochemical studies of Cenozoic high-K rocks in the Mangkang basin. Here, we firstly present two high-quality $^{40}Ar/^{39}Ar$ ages of the high-K rocks in the basin; then expound the eruption time of volcanic rocks and their stratigraphic division; and finally discuss the genesis of high-K rocks and their relation to coeval igneous rocks along the JRRS zone on the basis of the systematic studies of elemental and Pb-Sr-Nd isotopic geochemistry.

1 Sampling and analytical methods

The analyzed samples were collected from the Lawuxiang Formation in the Mangkang basin, Tibet and their detailed localities are shown in fig. 1. All of the samples for $^{40}Ar/^{39}Ar$ dating and geochemical analyzing are very fresh, slightly brick-red, compact and massive. They are characterized by porphyritic structures for overall rocks and crystallitic textures for their matrix. The phenocrysts include acidic plagioclase (An_{28-20}), sanidine and clinopyroxene.

The whole-rock grain samples were used to date their $^{40}Ar/^{39}Ar$ ages, due to difficult separation of enough K-bearing minerals for dating. The samples were washed and pulverized under clean environmental conditions, and amygdaloids were eliminated by handpicking. After drying, samples were pulverized to 0.3—0.4 mm grain size for $^{40}Ar/^{39}Ar$ dating or to less than 200 meshes for geochemical analyzing. 47.5 mg and 26.2 mg whole-rock grain samples of samples MK391-6 and MK75-2 were wrapped in the Sn foil and sealed in 6-mm-ID evacuated quartz-glass vials, together with Fish Canyon sanidine (FC-3) flux monitors, and irradiated in the Fort Reactor at the University of Michigan. J_0-factors were determined by a laser ablation technique. The irradiated samples were step-heated in a tantalum crucible within a double-vacuum furnace and analyzed by a VG 3600 or a MM 1200S mass spectrometer at the University of California, Los Angeles (UCLA). Argon blanks over the course of these analyses averaged $(2—5)\times10^{-16}$ mole ^{40}Ar in an atmospheric ratio. The monitor standard was the FC-3 sanidine (27.8 ± 0.3 Ma). All errors in table 1 are quoted at the 1-sigma level and do not include the uncertainty of the monitor age. The detailed analytical procedures were presented by ref.

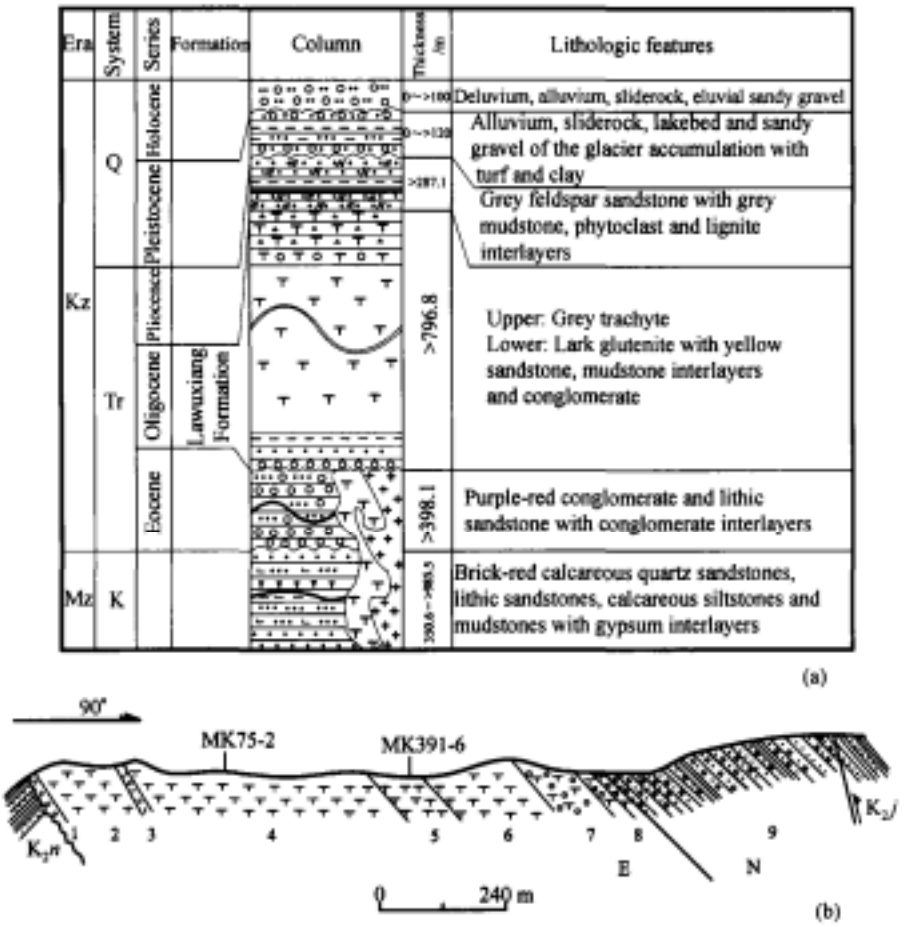

Fig. 2. Geologic column (a) and cross section (b) of the high-K rocks in the Lawuxiang Formation in the Mangkang basin, Tibet. In fig. 2(b), the strata division is described as below: 1, grey-yellow glutenite; 2, grey biotite trachyte; 3, light grey carbonated sedimentary tuff; 4, grey vitrophyric trachyte (Upper), light grey biotite trachyte (Lower); 5, light grey trachyte with few brecciated trachyte; 6, grey trachyte; 7, grey-purple trachytoid tuff-bearing lava; 8, grey-yellow volcanic brecciated tuff; 9, grey feldspar-quartz sandstone with interlayers of red mudstones.

[14]. Major elements were analyzed by wet chemistry at the Institute of Geochemistry, Chinese Academy of Sciences. Rare-earth and trace elements were measured by PE Elan 6000 ICP-MS at the Guangzhou Institute of Geochemistry, Chinese Academy of Sciences. Analytical uncertainties are ±1%—2% for major elements, ±5% for rare-earth elements, and ±5%—10% for trace elements, respectively. The detailed analytical procedures were given in ref. [15]. The analytical techniques of Nd-Sr-Pb isotopes were followed by ref. [7]. The Nd-Sr-Pb isotopic compositions of the high-K rocks were measured on a VG 354 mass spectrometer at the Guangzhou Institute of Geochemistry, Chinese Academy of Sciences. The $^{87}Sr/^{86}Sr$ and $^{143}Nd/^{144}Nd$ ratios were normalized to $^{86}Sr/^{88}Sr = 0.1194$ and $^{146}Nd/^{144}Nd = 0.7219$, respectively. During the course of this study, the NBS-987 gave an average $^{87}Sr/^{86}Sr$ ratio of 0.710283 ± 24 (2σ), the La Jolla and BCR-1 Standards gave mean $^{143}Nd/^{144}Nd$ ratios of 0.511861 ± 16 (2σ) and 0.512627 ± 14 (2σ), and the NBS-981 gave mean $^{206}Pb/^{204}Pb$, $^{207}Pb/^{204}Pb$ and $^{208}Pb/^{204}Pb$ ratios of 16.931 ± 0.009 (2σ), 15.484 ± 0.008 (2σ) and 36.643 ± 0.010 (2σ), respectively. The analytical errors are less than 0.005% for $^{143}Nd/^{144}Nd$ and $^{87}Sr/^{86}Sr$ ratios, and 0.08% for Pb isotopic ratios.

2 Result

2.1 $^{40}Ar/^{39}Ar$ chronological result

The result of $^{40}Ar/^{39}Ar$ dating for two high-K rocks of the Lawuxiang Formation is presented in ta-

Table 1 $^{40}Ar/^{39}Ar$ isotopic compositions of Cenozoic high-K volcanic rocks in the Mangkang basin, Tibet

Step	Temperature /℃	$^{40}Ar/^{39}Ar$	$^{36}Ar/^{39}Ar$	$^{37}Ar/^{39}Ar$	$^{38}Ar/^{39}Ar$	^{39}Ar /mole	^{39}Ar released (%)	$\%^{40}Ar^*$	$^{40}Ar^*/^{39}Ar_K$	Apparent age /Ma (± 1σ)
MK391-6, Weight = 47.5 mg, Whole rock, J_0 = 0.006929										
1	600	4.426	1.95×10^{-1}	4.75×10^{-1}	5.05×10^{-3}	4.87×10^{-13}	13.20	66.5	2.94	36.4 ± 0.2
2	700	3.941	2.17×10^{-2}	4.10×10^{-1}	3.84×10^{-5}	7.70×10^{-13}	34.00	71.3	2.81	34.8 ± 0.1
3	800	3.180	2.01×10^{-2}	5.89×10^{-2}	1.47×10^{-3}	4.05×10^{-13}	44.90	85.7	2.73	33.8 ± 0.1
4	850	3.400	2.22×10^{-2}	4.90×10^{-2}	2.14×10^{-5}	3.67×10^{-13}	54.80	80.7	2.75	34.0 ± 0.1
5	900	3.763	2.66×10^{-2}	5.56×10^{-2}	4.78×10^{-3}	2.18×10^{-13}	60.80	61.9	2.33	28.9 ± 0.4
6	950	3.426	-1.39×10^{-4}	-7.54×10^{-4}	3.01×10^{-3}	1.62×10^{-13}	65.10	73.2	2.51	31.1 ± 0.8
7	1000	3.160	8.23×10^{-3}	2.73×10^{-2}	1.23×10^{-5}	4.96×10^{-13}	78.60	87.8	2.77	34.4 ± 0.2
8	1050	3.294	2.38×10^{-2}	5.58×10^{-2}	1.91×10^{-3}	3.97×10^{-13}	89.30	82.2	2.71	33.6 ± 0.1
9	1100	3.548	4.38×10^{-2}	9.25×10^{-2}	2.76×10^{-3}	2.43×10^{-13}	95.90	76.4	2.71	33.6 ± 0.2
10	1350	3.832	6.95×10^{-2}	3.04×10^{-1}	3.67×10^{-3}	1.53×10^{-13}	100.00	71.6	2.75	34.0 ± 0.3
MK75-2, Weight = 26.2 mg, Whole rock, J_0 = 0.007520										
1	500	3.389	5.1×10^{-2}	1.96×10^{-1}	6.29×10^{-3}	6.94×10^{-14}	2.09	44.76	1.52	20.5 ± 0.2
2	600	2.302	1.3×10^{-2}	3.38×10^{-1}	1.35×10^{-3}	3.00×10^{-13}	11.13	82.66	1.90	25.7 ± 0.1
3	700	2.667	1.3×10^{-2}	4.01×10^{-1}	1.30×10^{-3}	7.68×10^{-13}	34.24	85.74	2.29	30.8 ± 0.1
4	750	2.572	1.3×10^{-2}	3.82×10^{-1}	1.14×10^{-4}	6.62×10^{-13}	54.19	97.73	2.52	33.8 ± 0.1
5	800	2.645	1.4×10^{-2}	3.40×10^{-2}	8.70×10^{-5}	5.08×10^{-13}	69.47	98.11	2.60	34.9 ± 0.1
6	850	2.656	1.6×10^{-2}	3.88×10^{-2}	9.69×10^{-5}	3.29×10^{-13}	79.38	97.99	2.61	35.0 ± 0.1
7	900	2.668	2.1×10^{-2}	5.47×10^{-2}	1.72×10^{-4}	2.12×10^{-13}	85.76	97.23	2.60	34.9 ± 0.1
8	950	2.658	3.4×10^{-2}	7.31×10^{-2}	3.17×10^{-4}	1.25×10^{-13}	89.51	95.62	2.55	34.2 ± 0.1
9	1000	2.613	4.9×10^{-2}	1.03×10^{-1}	4.34×10^{-4}	8.90×10^{-14}	92.20	94.26	2.47	33.2 ± 0.1
10	1100	2.633	6.7×10^{-2}	2.30×10^{-1}	7.57×10^{-4}	1.45×10^{-13}	96.55	91.12	2.40	32.3 ± 0.1
11	1200	2.848	1.4×10^{-1}	4.82×10^{-1}	1.46×10^{-3}	9.93×10^{-14}	99.54	85.16	2.43	32.7 ± 0.1
12	1350	3.795	7.5×10^{-1}	3.12	7.52×10^{-3}	1.52×10^{-14}	99.99	46.80	1.79	24.2 ± 0.2

ble 1. Their corresponding inverse isochrons and plateau ages are plotted in fig. 3. Ten steps were step-heated and measured for sample MK391-6. A high apparent age of (36.4 ± 0.2 Ma) appeared in step 1 but with lower ^{39}Ar (13.2%) and radiogenic ^{40}Ar (66.5%). Their apparent ages of steps 2—10 are nearly identical within 2-sigma errors. Thus, they yield a good age plateau of 33.7 ± 0.2 Ma (fig. 3(b)). The apparent ages of steps 5—6 are lower than their adjacent plateaus, which are related to the low released ^{39}Ar (10.3%) and high analytical errors. In the $^{36}Ar/^{40}Ar$-$^{39}Ar/^{40}Ar$ diagram (fig. 3(a)), the Ar isotopic data of ten steps define a relatively good inverse isochron of 32.8 ± 0.1 Ma with an initial $^{40}Ar/^{39}Ar$ ratio of 340.2, indicating existence of excess argon.

In order to overcome the effect of excess argon, we adopted the inverse isochron of 32.8 ± 0.1 Ma to discuss the time of the high-K rocks. Owing to their rapid cooling, the $^{40}Ar/^{39}Ar$ inverse isochron age should record the eruption time of high-K magma.

12 steps were measured for sample MK75-2, and its result is basically consistent with that of sample MK391-6. Two relatively low apparent ages of 20.5 ± 0.2 Ma and 25.7 ± 0.1 Ma appeared in steps 1 and 2 with two low released ^{39}Ar of 2.09% and 11.3%. Owing to the identical apparent ages of steps 4—11 within 2-sigma errors, an age plateau of 33.3 ± 0.1Ma with 65% total released ^{39}Ar is yielded for steps 4—11 (fig. 3(d)). The Ar isotopic data of steps 4—11 yield a relatively poor inverse isochron of 34.8 ± 0.4 Ma with

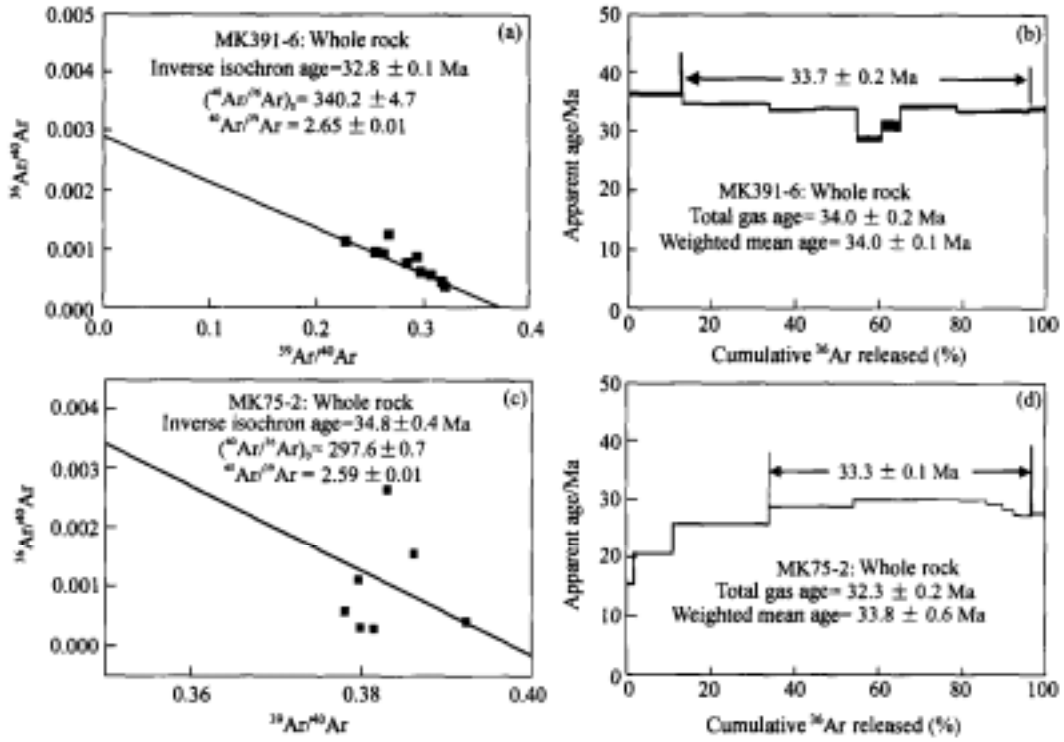

Fig. 3. $^{40}Ar/^{39}Ar$ inverse isochrons (a) and age plateaus (b) for high-K volcanic rocks in the Mangkang basin, Tibet.

an initial $^{40}Ar/^{36}Ar$ ratio of 297.6, indicating existence of a little excess argon. Thus, the plateau age may reflect the time of the high-K magmatism (fig. 3(c)).

2.2 Elemental geochemistry

The analyses of major, rare-earth and trace elements for 16 high-K rocks are presented in tables 2 and 3, respectively. In the SiO_2-K_2O diagram[16] (fig. 4(a)), the data are plotted in the area of ultrahigh potassic-shoshonitic rock series, implying that they are evidently enriched in K. On the TAS diagram [16] (fig. 4(b)), the data drop in the field of trachytes and trachydacites. Due to Q>20 for samples MK75-2, MK75-7 and MK391-5, they belong high-K trachydacites, and the other are high-K trachytes. The high-K rocks are characterized by low TiO_2 (<0.8%), P_2O_5 (<0.3%) and FeO* (< 3.81%), and high Na_2O (1.7%—3.7%) and K_2O (4.6%—6.5%)(table 2).

In the REE pattern diagram (fig. 5(a)), their pattern curves are a rightward steep incline [$(La/Lu)_N$ = 18.33—55.12] and characterized by intensive enrichment in LREE (=216.9—461.1 μg/g), no depletion in HREE [$(Gd/Lu)_N$ = 2.40—4.57], relatively low HREE (=13.2—27.4 μg/g), weakly negative Eu anomalies (δEu = 0.77—0.99) and very high total REE (ΣREE = 235.1—479.9 μg/g). In the multi-element spidergrams normalized by the McDonough's primitive mantle value (fig. 5(b)), they have consistent patterns, i.e., intensive enrichment in LILEs such as Rb, Ba, Th, U and K, and pronounced negative anomalies in HFSE such as Nb, Ta, Ti and P.

2.3 Isotopic geochemistry

The Pb-Sr-Nd isotopic compositions of the high-K rocks in the Mangkang basin are listed in table 4. There is no distinct difference ($<10^{-5}$) between their measured and time-calibrated values for Cenozoic high-K rocks due to a short time scale. Thus, we directly adopt their measured values to discuss the geologic questions. They have high $^{87}Sr/^{86}Sr$ (0.706—0.710), $^{206}Pb/^{204}Pb$ (18.78—18.88), $^{207}Pb/^{204}Pb$ (15.67—15.71) and $^{208}Pb/^{204}Pb$ (38.93—39.98) ratios, but the more restricted range of the $^{143}Nd/^{144}Nd$ ratios (table 4).

Table 2 Analyses of major elements for Cenozoic high-K volcanic rocks in the Mangkang basin, Tibet (wt %)

Sample	MK391-2	MK391-3	MK391-4	MK391-5	MK391-6	MK391-7	MK391-8	MK391-9
SiO_2	62.06	61.90	62.56	67.20	62.48	63.57	61.78	62.14
TiO_2	0.63	0.62	0.51	0.64	0.54	0.65	0.60	0.54
Al_2O_3	15.45	15.63	15.42	16.48	15.25	15.18	15.24	15.22
FeO*	3.46	3.39	3.38	2.36	3.36	3.47	3.40	3.64
MnO	0.08	0.08	0.07	0.03	0.07	0.07	0.07	0.12
MgO	2.13	2.53	2.30	0.41	2.59	1.44	2.23	1.67
CaO	5.19	5.62	4.92	2.59	5.47	5.11	6.47	6.08
Na_2O	3.60	3.22	3.27	1.71	2.88	3.36	3.01	2.95
K_2O	4.94	4.66	5.08	6.36	4.89	4.86	4.92	5.39
P_2O_5	0.21	0.25	0.17	0.27	0.26	0.15	0.23	0.27
CO_2	1.18	1.10	1.10	0.77	1.08	1.06	1.16	1.21
H_2O^+	0.87	0.83	0.89	0.88	0.79	0.89	0.68	0.68
H_2O^-	0.22	0.18	0.33	0.28	0.34	0.21	0.23	0.12
Total	100.00	100.00	100.00	100.00	100.00	100.00	100.00	100.00
Sample	MK391-10	MK391-11	MK391-12	MK391-13	MK392-1	MK75-2	MK75-5	MK75-7
SiO_2	61.50	63.14	60.75	61.68	62.90	65.98	62.63	67.26
TiO_2	0.57	0.54	0.54	0.58	0.59	0.76	0.77	0.67
Al_2O_3	15.28	15.84	15.18	15.59	15.10	16.17	15.51	16.31
FeO*	3.73	3.50	3.46	3.41	3.55	2.20	5.57	1.03
MnO	0.07	0.09	0.07	0.08	0.07	0.03	0.05	0.01
MgO	2.29	0.82	2.98	1.02	1.80	0.41	0.37	0.26
CaO	6.67	5.13	6.42	6.49	5.43	4.29	4.88	2.95
Na_2O	3.13	3.29	3.52	3.45	3.49	1.97	2.62	3.37
K_2O	4.50	5.38	4.80	5.38	4.87	5.78	5.31	5.73
P_2O_5	0.25	0.17	0.26	0.26	0.20	0.29	0.24	0.27
CO_2	1.25	1.05	1.32	1.29	1.04	0.96	1.14	0.86
H_2O^+	0.63	0.85	0.54	0.61	0.74	0.80	0.66	0.87
H_2O^-	0.13	0.21	0.16	0.17	0.23	0.35	0.25	0.40
Total	100.00	100.00	100.00	100.00	100.00	100.00	100.00	100.00

FeO* is the total iron.

3 Discussion and conclusion

3.1 Eruption time of the high-K rocks

Although many high-quality isotopic ages of Cenozoic high-K rocks in eastern Tibet were previously published[2,7,8,17−21] and Cenozoic two-pulse high-K magmatism at 40—28 Ma and 16—0 Ma were distinguished, no detailed report on the high-quality chronological data for high-K magmatism in the Mangkang basin is present so far. The high-K rocks in the Mangkang basin cut through the Cretaceous red strata (fig. 1), indicating that they were formed in a Cenozoic tectonic movement. The high-K trachytes were covered by Neogene sandstones (fig. 1) on the basis of fossil records and correlation of strata[11], implying that high-K trachytes were formed in Eogene. However, they were divided into the Neogene strata in the previous regional 1 : 200000 geologic report[11]. Our two newly obtained $^{40}Ar/^{39}Ar$ ages suggest that their eruption time is about 33 Ma, further corroborating the our inference on their formation time, i.e. the volcanic rocks in the Lawuxiang Formation were formed in Eogene.

3.2 Petrogenesis of high-K rocks

The high-K rocks in the Mangkang basin have

Table 3 Analyses of rare-earth and trace elements for Cenozoic high-K volcanic rocks in the Mangkang basin, Tibet (μg/g)

Sample	MK391-2	MK391-3	MK391-4	MK391-5	MK391-6	MK391-7	MK391-8	MK391-9
Li	31.23	40.68	40.26	62.51	32.33	27.68	31.18	27.17
Be	6.74	6.61	6.54	4.46	6.61	6.06	6.75	6.82
P	1793	1656	1567	1745	1565	1967	2019	1988
Sc	10.36	7.59	7.07	9.59	9.01	9.77	18.50	10.33
Ti	4239	3959	3870	4325	3876	4134	4176	3970
Rb	175	172	188	291	186	162	176	167
Sr	1988	1616	1612	765	1721	1403	1538	1618
Y	20.91	19.31	19.82	19.93	18.61	18.16	20.54	20.75
Zr	213.8	189.4	157.8	176.6	132.7	158.8	160.8	148.5
Nb	14.35	13.64	13.79	15.21	13.41	14.89	14.67	14.32
Ba	2116	1827	1916	1744	2102	1447	1736	1802
La	97.97	88.05	87.92	96.48	86.36	84.54	88.30	89.56
Ce	215.42	195.76	187.13	189.88	187.83	179.36	190.18	187.52
Pr	28.79	25.20	24.13	26.94	24.03	22.13	23.67	24.19
Nd	99.87	89.82	87.34	94.84	83.70	77.32	83.16	83.73
Sm	15.47	13.65	13.36	14.18	12.96	11.59	12.70	12.74
Eu	3.62	3.35	3.31	3.31	3.20	2.72	3.11	3.09
Gd	8.22	7.53	7.63	7.36	7.06	5.62	6.22	6.25
Tb	1.07	0.97	0.95	0.99	0.92	0.75	0.87	0.86
Dy	4.57	4.13	4.09	4.23	3.97	3.32	3.81	3.79
Ho	0.75	0.71	0.69	0.71	0.66	0.57	0.65	0.64
Er	2.07	1.93	1.87	1.95	1.78	1.50	1.75	1.74
Tm	0.25	0.23	0.22	0.23	0.22	0.18	0.21	0.21
Yb	1.57	1.45	1.38	1.41	1.33	1.10	1.29	1.26
Lu	0.22	0.21	0.19	0.20	0.19	0.16	0.19	0.19
Hf	5.73	5.11	4.49	5.01	4.04	3.65	3.96	3.62
Ta	1.02	0.95	0.96	1.08	0.96	0.84	0.88	0.85
Th	36.53	35.42	34.07	38.74	34.37	29.49	31.37	30.31
U	8.44	8.85	7.18	11.53	8.19	7.12	7.54	7.99
Sample	MK391-10	MK391-11	MK391-12	MK391-13	MK392-4	MK75-2	MK75-5	MK75-7
Li	41.69	30.25	28.12	27.83	30.80	29.68	18.47	23.09
Be	7.08	7.23	6.84	7.21	6.12	3.65	3.30	4.43
P	2085	2039	2080	2268	1092	1659	1416	1170
Sc	11.58	9.86	11.55	13.36	9.90	11.09	9.66	6.79
Ti	4201	4222	4377	4263	3953	5377	5728	4561
Rb	165	184	167	169	154	178	157	188
Sr	1735	1765	1911	1846	1742	1013	1135	1437
Y	21.19	19.02	20.21	21.89	20.24	29.21	49.27	27.26
Zr	144.1	133.6	133.0	230.7	202.3	253.3	301.6	134.6
Nb	14.95	16.03	15.48	14.55	13.94	20.47	18.94	20.00
Ba	1661	1842	1779	2471	1717	1559	1988	2159
La	90.68	91.28	91.23	93.93	88.82	54.89	62.64	61.00
Ce	200.82	200.14	201.32	212.18	194.22	99.59	119.89	120.08
Pr	25.24	24.99	25.11	26.52	24.36	11.56	16.14	14.46
Nd	88.38	86.50	87.58	92.95	84.48	41.39	61.20	51.99
Sm	13.63	13.15	13.26	14.11	12.88	7.62	11.40	9.15
Eu	3.14	3.09	3.10	3.39	3.08	1.87	2.65	2.27
Gd	6.52	6.14	6.25	6.78	6.18	6.00	9.18	6.40
Tb	0.91	0.87	0.90	0.96	0.87	0.94	1.38	0.93
Dy	3.97	3.74	3.85	4.13	3.78	4.98	7.38	4.74
Ho	0.68	0.63	0.64	0.70	0.65	0.93	1.45	0.85
Er	1.78	1.67	1.72	1.88	1.72	2.53	3.93	2.28
Tm	0.22	0.20	0.21	0.24	0.21	0.34	0.52	0.30
Yb	1.32	1.18	1.28	1.42	1.31	2.10	3.07	1.82
Lu	0.20	0.17	0.18	0.21	0.19	0.31	0.46	0.26
Hf	3.67	3.51	3.63	5.29	4.92	6.28	7.15	3.37
Ta	0.91	0.98	0.95	0.93	0.86	1.43	1.29	1.49
Th	31.18	33.88	32.63	32.62	31.80	16.58	20.33	26.72
U	7.77	7.03	9.69	7.51	7.34	2.35	3.93	6.59

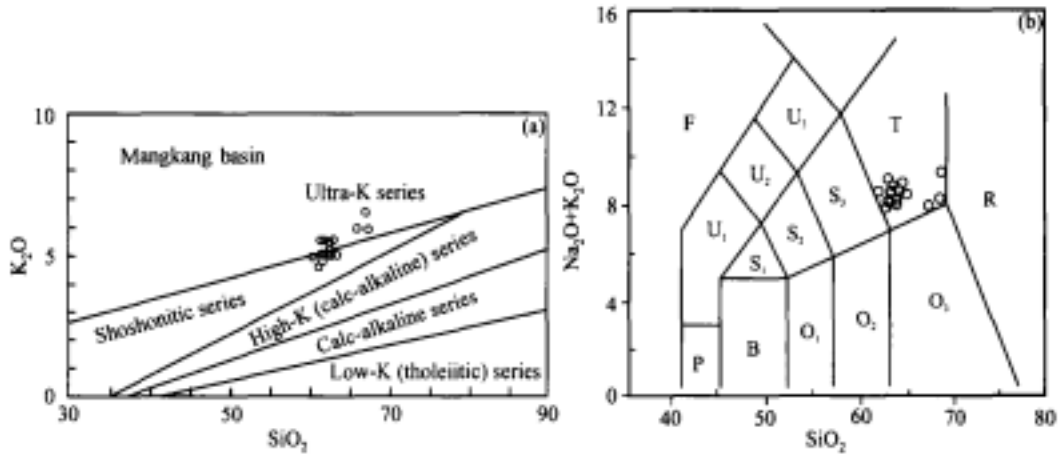

Fig. 4. Si-K (a) and TAS (b) diagrams for Cenozoic high-K volcanic rocks in the Mangkang basin, Tibet (The original diagram after ref. [16]). F, Foidite; P, picobasalt; B, basalt; T, trachyte (Q<20%) and trachydacite (Q>20%); U1, tephrite and basanite; U2, phonotephrite; U3, tephriphonolite; Q1, basaltic andesite; Q2, andesite; Q3, dacite; S1, trachybasalt; S2, basaltic trachyandesite; S3, trachyandesite; R, rhyolite.

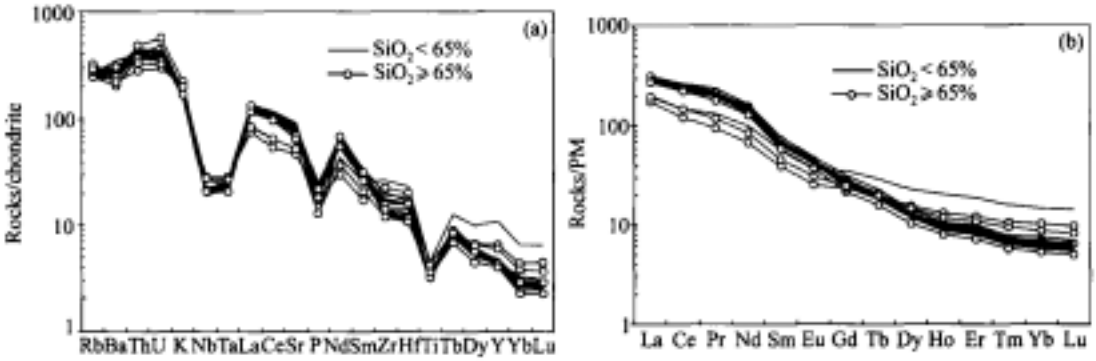

Fig. 5. REE patterns (a) and multi-element spidergrams (b) for Cenozoic high-K volcanic rocks in the Mangkang basin, Tibet (The primordial mantle value was cited from ref. [16]).

Table 4 Pb-Sr-Nd isotopic compositions of Cenozoic high-K volcanic rocks in the Mangkang basin, Tibet

Sample	$^{87}Sr/^{86}Sr$ (±2σ)	$^{143}Nd/^{144}Nd$ (±2σ)	$^{206}Pb/^{204}Pb$ (±2σ)	$^{207}Pb/^{206}Pb$ (±2σ)	$^{208}Pb/^{204}Pb$ (±2σ)
MK391-2	0.706434 ± 24	0.512457 ± 18	18.875 ± 07	15.671 ± 06	38.949 ± 10
MK391-2*	0.705955 ± 30	0.512558 ± 20	18.854 ± 12	15.717 ± 19	39.121 ± 17
MK391-10	0.706123 ± 24	0.512566 ± 14	18.776 ± 09	15.598 ± 07	39.186 ± 19
MK391-13	0.705904 ± 18	0.512550 ± 20	18.854 ± 06	15.677 ± 05	39.975 ± 18
MK391-6	0.707160 ± 24	0.512552 ± 16	18.789 ± 09	15.687 ± 08	38.950 ± 18
NBS-987	0.710283 ± 24				
NBS-981			16.931 ± 09	15.484 ± 08	36.643 ± 10
La Jolla		0.511842 ± 16			
BCR-1		0.512627 ± 14			

The samples with the symbol * are duplicate. NBS-987, NBS-981, La Jolla and BCR are four international standards.

the same tectonic setting as those of early pulse in eastern Tibet, i.e., transpression[7,8]. Wang J. H. et al.[7,8] considered that the early-pulse high-K magma in eastern Tibet originated from partial melting of an overlying mantle wedge, which was metasomated by an infiltration fluid from a subducted continental slab.

In the elemental variation diagram (fig. 6), there are a negative correlation between SiO_2 and CaO, or SiO_2 and $Mg^{\#}$, and a weakly negative correlation between SiO_2 and FeO*, but a positive correlation be-

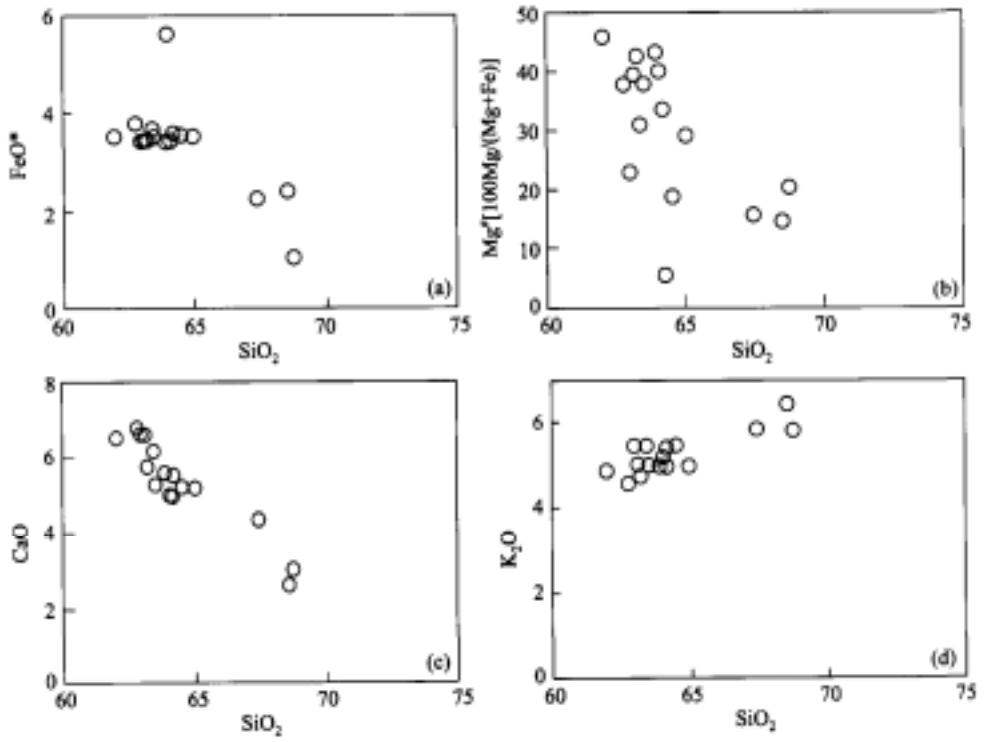

Fig. 6. Elemental variation diagrams for high-K volcanic rocks in the Lawuxiang Formation.

tween SiO_2 and K_2O. We have made the REE numerical modeling for the samples with SiO_2<65%, if adopting a standard intermediate igneous rock as the primitive magma, and its REE partition coefficients of plagioclase, clinopyroxene and garnet[16]. The REE modeling suggests that the REE patterns of the residual magma would nearly be similar to those with SiO_2 < 65% in the Mangkang basin if a standard intermediate magma undergoes 72% fractional crystallization with a crystallized residual of clinopyroxene (60%), plagioclase (25%) and garnet (15%), suggesting the onset of fractional crystallization of clinopyroxene, plagioclase and garnet in the evolution of magma. This conclusion is consistent not only with the occurrence of the phenocrysts or megacrysts of plagioclase and clinopyroxene in the high-K rocks in the Mangkang basin[12,13], but also with petrographical observations that the garnet megacrysts exist in the high-K rocks in the adjacent region[12,13]. Weakly negative Eu anomalies in the REE patterns also can be interpreted on the basis of the above facts.

The minimum of the crystallization temperatures of plagioclase megacrysts is 950℃ in the high-K rocks in the Mangkang basin[12], indicating that the initial crystallization temperature is higher than 950℃. The K-rich characteristic of plagioclase megacrysts in the high-K rocks couples with their host rock [13]. The pronounced negative anomalies in HFSEs such as Nb, Ta, Ti and P indicate an input of subduction-related components[7,22]. The high $^{87}Sr/^{86}Sr$ and low $^{143}Nd/^{144}Nd$ isotopic signatures require mantle sources with a time-integrated history of enrichment in LREE and Rb. The most plausible explanation is to ascribe these combined trace-elemental and isotopic observations to a metasomatized subcontinental lithospheric mantle source before the onset of partial melting that led to high-K magmatism[23,24]. Combining with their characteristics of isotopes and trace elements (e.g., high Δ7/4Pb, Δ8/4Pb, Th/Ta and Ba/Nb, negative Ce anomalies, and high Sr and Ba), we consider that the high-K magma was derived from partial melting of an enriched mantle source reworked by a Tethys oceanic crust, due to Cenozoic large-scale continental subduction. In the Sr-Nd diagram (fig. 7), their Sr-Nd iso-

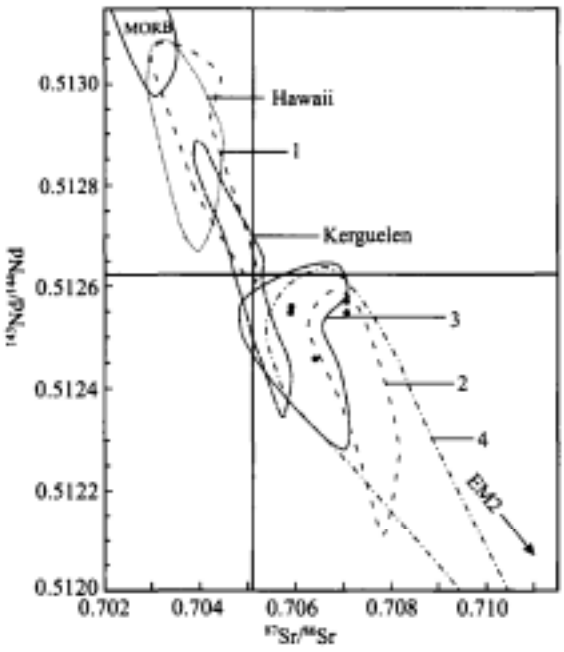

Fig. 7. Sr-Nd isotopic correlation diagram. (1) and (2) quoted from ref. [7], (3) from ref. [3], and (4) from ref. [25].

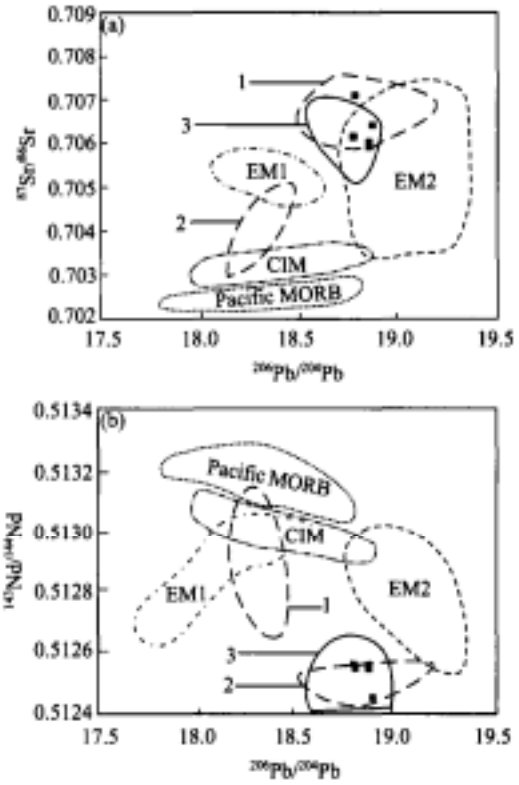

Fig. 8. Sr-Pb (a) and Nd-Pb (b) isotopic correlation diagrams (The labels are the same as in fig. 7).

topic compositions lie in the enriched extension of the mantle array but fall far outside the fields of MORB and Hawaiian basalts. In the Sr-Pb and Nd-Pb diagrams (fig. 8), their isotopic data also plot outside the field of oceanic basalts, indicating the high-K magma may be derived from an EM2 mantle. In the Pb-Pb diagrams (fig. 9), the Pb isotopic data are plotted above the NHRL. Combined with refs. [7, 8], it shows that the source in composition appear a trend from EM1 to EM2.

Summarily, the high-K rocks in the Mangkang basin as a part of eastern Tibet have certain commonness in many aspects such as identical tectonic setting, discontinuous zonal distribution, basically uniform geochemical characteristics formed during a short time interval, but they have some particularities if compared with those in the north, south and medium segments in the JRRS belt, i.e., firstly, the formation time is slightly earlier than that of the Red River region in

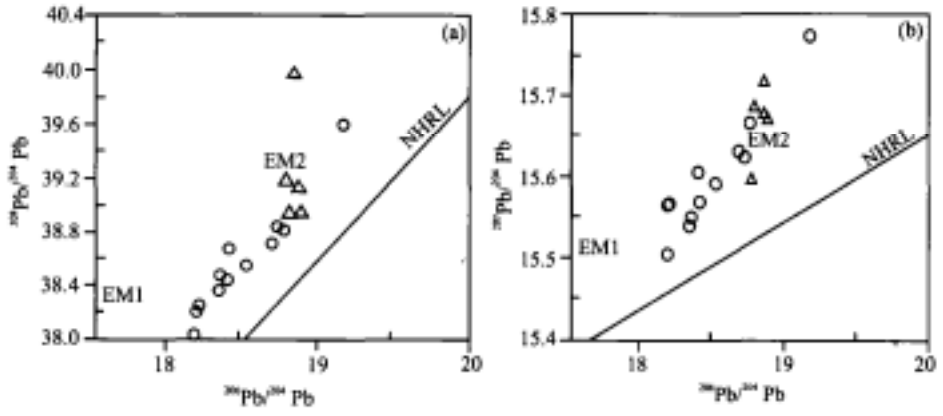

Fig. 9. $^{208}Pb/^{204}Pb$-$^{206}Pb/^{204}Pb$ (a) and $^{207}Pb/^{204}Pb$-$^{206}Pb/^{204}Pb$ (b) isotopic correlation diagrams (NHRL is a Northern Hemisphere reference line).

the south segment, slightly late than that of the Nangqian-Xialaxiu region in the north segment, and contemporary with that of the Jianchuan-Dali region in the medium segment. Secondly, they just occur in a volcanic litho-facies in the Mangkang basin, but the volcanic, shallow-level intrusive, dike and pipe-like volcanic litho-facies appear in the wholesale belt. Compositionally, they mainly are intermediate (a few acid) rocks, but for the wholesale belt, all occur from acidic to ultrabasic. The Nd-Sr isotopic compositions of high-K rocks in the Mangkang basin are similar with those in the medium and south segments, but different from the north segment, i.e., lower $^{87}Sr/^{86}Sr$ ratios and higher $^{143}Nd/^{144}Nd$ ratio in the Nangqian- Xialaxiu region.

3.3 Conclusion

The high-K volcanic rocks of the Lawuxiang Formation in eastern Tibet were formed at 32.8—33.3 Ma, and belong to Eogene strata. The high-K magma was derived from partial melting of an enriched EM2 mantle source reworked by a Tethys oceanic crust, due to Cenozoic large-scale continental subduction. Compositionally, the source of high-K rocks in the wholly Tibet an Plateau appear a trend from EM1 to EM2.

Acknowledgements This work was jointly supported by the National Natural Science Foundation of China (Grant No. 49972026), the Guangdong Natural Science Foundation (Grant No. 990531), the project of the Chinese Academy of Sciences (Grant No. KZCX2-SW-117), the Chinese National Key Project for Basic Research (Grant No. G1998040807) and US NSF.

References

1. Zhang, Y. Q., Xie, Y. W., Tu, G. C., Preliminary studies of the alkali-rich intrusive rocks in the Ailaoshan-Jinshajiang belt and its bearing on rift tectonics, Acta Petrol. Sin. (in Chinese), 1987, (3): 17—25.
2. Pan, G. T., Wang, P. S., Xu, Y. R. et al., Cenozoic tectonic evolution of Qinghai-Xizang Plateau (in Chinese), Beijing: Geological Publishing House, 1990, 32—70.
3. Zhang, Y. Q., Xie, Y. W., Geochronology of Ailaoshan-Jinshajiang alkali-rich intrusive rocks and their Sr and Nd isotopic characteristics, Sci. China, Ser. D, 1997, 40(5): 522—528.
4. Deng, W. M., Huang, X., Zhong, D. L., Alkali-rich porphyry and its relation with intraplate deformation of the north part of the Jinsha River belt in western Yunnan, China, Sci. China, Ser. D, 1998, 41(3): 297—315.
5. Deng, W. M., Cenozoic Intraplate Volcanic Rocks in the Northern Qinghai-Xizang Plateau (in Chinese), Beijing: Geological Publishing House, 1998.
6. Deng, W. M., Sun, H. J., Zhang, Y. Q., K-Ar age of Cenozoic volcanic rocks in the Nangqen Basin, Qinghai Province and its geological significance, Chinese Sci. Bull., 2000, 45(11): 1014—1019.
7. Wang, J. H., Yin, A., Harrison, T. M. et al., A tectonic model for Cenozoic igneous activities in the eastern Indo-Asian collision zone, Earth Planet Sci. Lett., 2001, 188: 123—133.
8. Wang, J. H., Yin, A. Harrison, T. M. et al., Thermochronological constraints on two pulses of Cenozoic high-K magmatism in eastern Tibet, Sci. China, Ser. D, 2002, 32(7): 529—537.
9. Morley, C. K., A tectonic model for the Tertiary evolution of strike-slip faults and rifts basins in SE Asia, Tectonophysics, 2002, 347(4): 189—215.
10. Wang, E., Burchfiel, B. C., Late Cenozoic Xiangshuihe-Xiaojiang, Red River and Dali fault systems of southwestern Sichuan and central Yunnan, China, Geol. Soc. Am. Spec. Paper 327, GSA, 1998, 1—108.
11. The Bureau of Geology and Mineral Resources (Tibet), The Regional Geological Map of the Mangkang in Tibet (1 : 200,000) and Geological Report (in Chinese), Beijing: Geological Publishing House, 1991.
12. Lai, S. C., Mineral chemistry of Cenozoic volcanic rocks in Yumen, Hoh Xil and Mangkang lithodistricts, Qinghai-Tibet Plateau and its petrologigcal significance, J. NW. Univ. (Natural Sci. edition), 1995, 25(6): 701—704.
13. Lai, S. C., Features of megacrysts in Cenozoic volcanic rocks from Hoh Xil and Mangkang Lithodistricts, Qinghai-Tibet Plateau, Acta Mineral. Sin., 1999, 19(2): 236—244.
14. Harrison, T. M., Leloup, P. H., Ryerson, F. J. et al., Diachronous initiation of transtension along the Ailao Shan-Red River shear zone, Yunnan and Vietnam (eds. Yin, A., Harrison, T. M.), The tectonic evolution of Asia, New York: Cambridge University Press, 1996: 208—226.
15. Liu, Y., Liu, H. C., Li, X. H., Simultaneous and precise determination of 40 trace elements in rocks samples using ICP-MS, Geochimica, 1996, 25(6): 552—558.
16. Rollinson, H. R., Using geochemical data: Evaluation, Presentation and Interpretation, London: Longman Group UK Ltd, 1993.
17. Schärer, U., Zhang, L. S., Tapponnier, P., Duration of strike-slip movements in the large shear zones: The Red River belt, China, Earth Planet Sci. Lett., 1994, 126: 379-397.
18. Chung, S. L., Lee, T. Y., Lo, C. H. et al., Intraplate extension prior to continental extrusion along the Ailao Shan-Red River shear zone, Geology, 1997, 25: 311—314.
19. Chung, S. L., Lo, C. H., Lee, T. Y. et al., Diachronous uplift of the Tibetan Plateau starting 40 Myr ago, Nature, 1998, 394: 769—773.
20. Lee, T. Y., Lo, C. H., Chung, S. L. et al., $^{40}Ar/^{39}Ar$ dating result of Neogene basalt in Vietnam and its tectonic implication (eds.

Flower, M. F. J., Chung, S. L., Lo, C. H.), Mantle dynamics and plate interactions in east Asia, Geodynamatics 27, AGU, Washington DC, 1998, 317—330.

21. Zhang, L. S., Schärer, U., Age and origin of magmatism along the Cenozoic Red River shear belt, Contrib. Mineral. Petrol., 1999, 134: 67—85.
22. Miller, C., Schuster, R., Klötzli, U. et al., Post-collisional potassic and ultrapotassic activities in SW Tibet: Geochemical and Sr-Nd-Pb-O isotopic constraints for mantle source characteristics and petrogenesis, J. Petrol., 1999, 40: 1399—1424.
23. Turner, S., Arnaud, N., Liu, J. Q. et al., Post-collision, shoshonitic volcanism on the Tibetan Plateau: Implications for convective thinning of the lithosphere and the source of ocean island basalts, J. Petrol., 1996, 37: 45-71.
24. Xie, G. H., Liu, C. Q., Masuda, A. et al., The geochemical characteristics of Cenozoic volcanic rocks in the area of Qinghai-Tibet Plateau: Evidence for existing of an ancient enriched mantle, The Age and Geochemistry of Cenozoic Volcanic Rocks in China (ed. Liu, R. X.) (in Chinese), Beijing: Seismological Press, 1992, 400—427.
25. Zhu, B. Q., Chen, Y. W., Chen, J. H., Lead isotope geochemistry of the urban environment in the Pearl River Delta, Applied Geochem., 2001, 16: 409—417.